Journal of Power Sources 196 (2011) 1248–1257

Contents lists available at ScienceDirect

Journal of Power Sources

journal homepage: www.elsevier.com/locate/jpowsour

Stochastic reconstruction and a scaling method to determine effective transport coefficients of a proton exchange membrane fuel cell catalyst layer

R. Barbosa[a], J. Andaverde[b], B. Escobar[c], U. Cano[d,*]

[a] Centro de Investigación en Energía, UNAM, Privada Xochicalco S/N, 62580 Temixco, Mexico
[b] Centro de Investigación en Ingeniería y Ciencias Aplicadas, UAEM, Av. Universidad 1001, Col. Chamilpa, 62210 Cuernavaca, Mexico
[c] Instituto Tecnológico de Cancún, Av. Kabah 3, 77515 Cancún, Mexico
[d] Instituto de Investigaciones Eléctricas, Av. Reforma 113, col. Palmira, 62490 Cuernavaca, Mexico

ARTICLE INFO

Article history:
Received 25 May 2010
Received in revised form 4 August 2010
Accepted 5 August 2010
Available online 17 August 2010

Keywords:
Numerical simulation
Correlation functions
Heterogeneous media
Scaling method

ABSTRACT

This work uses a method for the stochastic reconstruction of catalyst layers (CLs) proposing a scaling method to determine effective transport properties in proton exchange membrane fuel cell (PEMFC). The algorithm that generates the numerical grid makes use of available information before and after manufacturing the CL. The structures so generated are characterized statistically by two-point correlation functions and by the resultant pore size distribution. As an example of this method, the continuity equation for charge transport is solved directly on the three-dimensional grid of finite control volumes (FCVs), to determine effective electrical and proton conductivities of different structures. The stochastic reconstruction and the electrical and proton conductivity of a 45 μm side size cubic sample of a CL, represented by more than 3.3×10^{12} FVCs were realized in a much shorter time compared with non-scaling methods.

Variables studied in an example of CL structure were: (i) volume fraction of dispersed electrolyte, (ii) total CL porosity and (iii) pore size distribution. Results for the conduction efficiency for this example are also presented.

1. Introduction

In the near future the world's energy demand will have to be supplied using energy sources different from fossil fuels. Within such scenario hydrogen fuel could be playing an important role as an energy vector [1]. On the other hand, due to its high efficiency and the potential of being used in a great variety of applications, proton exchange membrane fuel cell (PEMFC) is being a much studied and developed technology in the last two decades [2,3].

Within a PEMFC, a catalyst layer (CL) is a small and thin region where electrochemical reactions take place as well as many transport processes, which to a large extent determine its general performance [4,5]. The solid phase of this component is formed by an electronic conductor which also serves as a support for a nanostructured catalyst, which should be in contact with a dispersed ionic conductor (ionomer) to complete the reactions [6]. This CL needs to be porous to allow the access of reactant gases entering the cell, and to let water formed by reactions exit the cell either in a vapor or in a liquid phase [7,8]. The porous medium also provides a large active area available for larger reaction sites and the resultant larger current [8].

In a PEMFC the catalyst is typically platinum (Pt), the supporting material most commonly used is carbon (C), while the ionomer is a polymer named nafion®. These materials will be referred to as CL's primary components. In a PEMFC CL the reactant gases are transported from the border between CL and the so-called gas diffusion layer (GDL) up to the reacting catalytic sites through pores formed during fabrication between the primary components. While the catalyst has the role of promoting the proper electrochemical reactions, the carbon collects and conducts the produced electrons and the ionomer should conduct protons generated or consumed by the proper reaction.

Experimental observations at the micrometer scale suggest that the CL is formed by agglomerates in a porous matrix [6]. The concept of agglomerates has been developed some years ago for electrochemical systems and it has been extensively applied to PEMFC [9–12]. Nevertheless, obtaining information at the nanoscale is very difficult using present experimental characterization techniques, which do not allow for the capture of images at that scale without modifying the original structure [13,14]. This limitation has lead to the formulation of different theories. The most popular is the theory that considers agglomerates as small spheres covered with a thin layer of ionomer and an inside of Pt/C particles [15–18].

* Corresponding author.
Tel.: +52 777 3623811x7271; fax: +52 777 3623881x7271.
E-mail address: ucano@iie.org.mx (U. Cano).

0378-7753/$ – see front matter © 2010 Elsevier B.V. All rights reserved.
doi:10.1016/j.jpowsour.2010.08.033

The structure and composition of a PEMFC CL define this component as a random heterogeneous material. This heterogeneity arises from the fact that it is constituted by different phases, being "phase" an identifiable domain with its own particular properties that differentiate it from the rest of the other phases in the CL (i.e. voids, other solid material, gases or liquids).

Proportionality coefficients for mass, energy and charge transport in a heterogeneous material are significantly affected by the properties of the phases from which this is composed, by the volume fraction composition, and by the structure of such phases. For this reason, an effective transport coefficient (ETC) is defined for a heterogeneous material as a proportionality coefficient, which characterizes the domain of the material. For a randomly formed heterogeneous material with M phases, a general ETC, K_e is:

$$K_e = f(K_1, K_2, \ldots, K_M; \phi_1, \phi_2, \ldots, \phi_M; \Omega) \quad (1)$$

where subscript of variables indicates a respective phase, K is the proportionality constant for that phase, ϕ is the phase volume fraction and Ω is a microstructural information of the domain [19].

In literature there are different mathematical relationships to determine ETCs [20–22]. For example, Maxwell-Garnett [21] developed a relationship to determine optical properties for diluted dispersions of uniform spheres. Later, Bruggeman extends Maxwell's model to systems with random dispersions of spherical particles with an extended range size [22].

A more recent and powerful technique to determine effective properties of random heterogeneous materials, is the so-called "stochastic reconstruction", which first applications is attributed to Quiblier [23]. This technique is based on the computational generation of a mesh that characterizes the real microstructure of the heterogeneous material, mathematically described by statistical functions referred to as "correlation functions". Torquato [19] offers a methodology to characterize microstructures, as well as fundamental theory to estimate effective properties. More recent works offer modifications to Torquato's methodology to optimize the quality in the stochastic reconstruction or to reduce convergence time during computing [24–27].

The right value of ETC is indispensable for an adequate numerical simulation of systems containing one or more components with characteristics of a heterogeneous media. An incorrect ETC value will alter the results and consequently it will provide a wrong interpretation of the transport phenomena.

On the other hand, PEMFC phenomena simulations have been of great interest in recent years due to the obvious advantages over experimental techniques: (1) lower research costs, (2) it is a powerful tool for the design of more efficient devices, and (3) it offers the possibility to better understand phenomena within the fuel cell in often unreachable places.

When the simulation objective is the prediction of gas flow field performance, it is common to assume the CL as a one-phase element [28–30]. Nevertheless, to detail the functioning of a CL, a mathematical approach has been used based on the assumption that a CL is a heterogeneous medium formed by agglomerates [11,31–33]. In this case, Bruggeman's approach is the most popular. The stochastic reconstruction has been successfully used in the simulation of a PEMFC CL. Wang et al. [34] proposed a direct numerical simulation (DNS) as a way to predict the CL's transport phenomena that take place at the micrometer scale. Unfortunately, the large number of control volumes required to detail the main elements that form the CL, in a computing domain that covers the whole electrode, makes DNS an expensive computation-wise method. Recently, Kim and Pitsch [17] proposed a "sphere-based simulated annealing" method, as well as the "lattice Boltzmann" method to reconstruct the microstructure of the CL in a PEMFC and to determine the effective diffusivity of the structure, respectively.

In this work a theoretical study of a PEMFC CL by the stochastic reconstruction of its microstructure and a scaling technique is presented. The scaling technique allows a significant reduction in computational resources needed for simulation. Scales are defined based on different observable structures at different order of magnitude scales. The reconstruction technique employed allows the use of information available before and after the manufacture of CLs. The so reconstructed structures are characterized with a two-point correlation function and its pore size distribution. Results obtained for the effective conductivity of theoretical samples with different nafion® content as well as different total porosity and pore size distribution are also presented. This work includes the following steps: (1) microstructure reconstruction at the different scale domains; (2) scaling strategy; (3) statistical characterization of the generated structures; and (4) analysis of ETCs by solving the charge transport equation. This technique can also be applied to evaluate the different structural theories.

2. Theory and calculation

In this section we describe the microstructural information and the perceptible scales of the CL. The mathematical analysis that conditions the grid generation (the statistical characterization and the ETC's determination) of a subdivided domain by n samples of inferior length scales is also presented.

2.1. Structural information and specific scales of CL in PEMFC

Although the nanometric scale information of CLs is limited, structural and compositional information does exist and it can be obtained before, during and after manufacturing the electrodes. Design parameters that are used and controlled before MEA's manufacturing typically include: (1) platinum load (γ_{Pt}) in mg Pt cm^{-2}; (2) ionomer load (β_N) which is a relation of nafion® weight to total electrode weight and (3) platinum to carbon weight ratio (θ_{Pt}), which is characteristic of the catalytic material synthesis. From such information and from other physical properties of its components (densities), volume fractions of phases in CL can be calculated.

On the other hand, the solid phase volume (V_S) of any mixture is equal to the total sum of individual phase mass (m) divided by the density (ρ) of each i element in the mixture, Eq. (2):

$$V_S = \sum \frac{m_i}{\rho_i} \quad (2)$$

Using design parameters (γ_{Pt}, β_N, θ_{Pt}) in Eq. (2) gives the volume occupied by each primary element in the solid phase of the CL. Eqs. (3), (4) and (5) can be used to calculate platinum (V_{Pt}), carbon (V_C) and nafion (V_N) volume, respectively:

$$V_{Pt} = \frac{V_S}{[(\beta_N(1+\theta_{Pt})/\theta_{Pt}\,\rho_N(1-\beta_N) + (1/\rho_{Pt}) + (1/\theta_{Pt}\,\rho_C)]\rho_{Pt}} \quad (3)$$

$$V_C = \left(\frac{V_{Pt}\,\rho_{Pt}}{\theta_{Pt}\,\rho_C}\right) \quad (4)$$

$$V_N = \left(\frac{\beta_N(1+\theta_{Pt})(V_{Pt}\,\rho_{Pt})}{(1-\beta_N)\theta_{Pt}\,\rho_N}\right) \quad (5)$$

where ρ_{Pt}, ρ_C and ρ_N are platinum, carbon and nafion densities, respectively.

On the other hand, Eq. (6) relates the electrode total porosity (Φ_T) with the solid phase volume (V_S) and the electrodes total volume (V_T)

$$\Phi_T = 1 - \frac{V_S}{V_T} = 1 - \frac{\sum m_i/\rho_i}{V_T} \quad (6)$$

Other important structural information that can be obtained before manufacturing the CL is the Pt and the C particle sizes. Pt is typi-

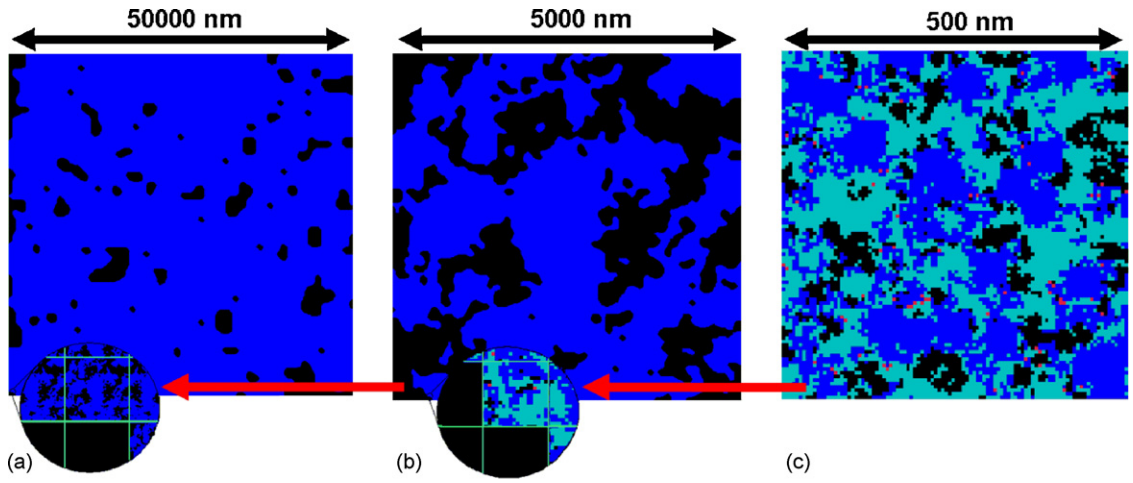

Fig. 1. Domains use to characterize a PEMFC CL at different scales: (a) "mesoporous" where the blue color represents the pseudo-solid phase while black the empty phase; (b) "agglomerate and micropores", the blue color represents the agglomerates while black the empty phase; (c) "inside an agglomerate" here, the Pt (~5 nm, in red), carbon agglomerate (~50 nm, in blue) and ionomer (in light blue) can be distinguished. (For interpretation of the references to color in this figure legend, the reader is referred to the web version of the article.)

cally supported on C during catalyst material synthesis, i.e. before manufacture of CL, which also conditions the final electrode structure. The CL manufacturing method determines to certain degree its final structure, but such effect is not considered in this work. After manufacturing the CL and using modern techniques such as porosimetry and high resolution microscopy, one can get approximate size and structure of agglomerates, total porosity and size pore distribution. In this work we assumed that physical properties of primary components are not modified during manufacture. This assumption is valid when the composite material is fabricated using physical techniques in which chemical reactions do not occur which is normally the case in state of the art MEA's manufacturing techniques. Thin layer electrode manufacturing techniques [35], are among the most popular approaches used. Many variants to these techniques are reported in literature [36–40], but most of them involve mixing Pt/C and the ionomer in a liquid solution that is physically homogenized. The resultant mixture (catalytic ink) is then deposited on a substrate. It is important to say that, regardless the catalytic ink composition and type of substrate, the primary elements are effectively distributed randomly (given a complete homogenization stage).

During the manufacturing process of CLs agglomerates form composed of primary components plus a number of pores of a variety of sizes. These structural features of the CL allow us to define internal substructures at different scale levels, and with that we can establish a scaling strategy for numerical simulation.

One way to explain these apparent structural changes at different scale levels is by picturing yourself at infinite getting closer and closer into the CL structure. When the vision scale is ~50,000 nm, one will observe a homogeneous dispersion of mesoporous structure; for a scale of ~5000 nm and focusing areas where mesoporous are absent, the structure is defined by agglomerates and micropores; finally at a vision scale of ~500 nm and focusing at an agglomerate the observer will distinguish a structure formed by a random distribution of Pt/C particles, ionomer and probably nanometric pores. This last observation actually is a hypothesis due to the fact that available information from experimental techniques is limited at this scale, nevertheless it is a more realistic hypothesis compared to the most commonly used theory where agglomerates are considered spheres with Pt/C particles inside and covered with a thin layer of ionomer on the outside.

In Fig. 1 the previously described scales are graphically represented for a PEMFC CL. Fig. 1(a) refers to the so-called "mesoporous" scale with a ~50,000 nm domain, where the blue color represents the pseudo-solid phase while black the empty phase; Fig. 1(b) represents the "agglomerate and micropores" scale with a ~5000 nm domain, here the blue color represents the agglomerates while black the empty phase; finally Fig. 1(c) refers to the "inside an agglomerate" scale with a ~500 nm domain where the primary elements, Pt (~5 nm, in red), carbon agglomerate (~50 nm, in blue) and ionomer (in light blue) can be distinguished.

In this work the sample that simulates the inside of agglomerate is the only one that contains the primary elements, while samples of ascending scale contain only the sample of the immediately smaller scale and its corresponding porosity. We define the relative porosity as the volume fraction occupied by the empty spaces at that scale, ignoring that the pseudo-solid phase (or smaller scale) also contains some porosity. The volume fractions of the solid phase of each sample at different scales can be related mathematically by Eq. (7),

$$S_R = \prod_1^n S_i \tag{7}$$

where S_R is the volume fraction of the solid phase in the entire CL, S_i is the individual volume fraction of the solid phase in each of the samples. By substitution of Eq. (6) in Eq. (7) we can obtain a mathematical relation that calculates the "total" porosity in the complete CL with the relative porosities of each of the samples (Eq. (8)),

$$\Phi_T = 1 - \prod_1^n (1 - \Phi_i) \tag{8}$$

where Φ_T represents the total porosity of the complete CL and Φ_i the relative porosity of each individual samples.

2.2. Structural reconstruction algorithm

Although the "annealing method" [19,24–27] can be applied, for simplicity, our reconstruction method considers only one filter: the one-point correlation function (volume fraction). Fig. 2 presents a general flow diagram of the microstructural reconstruction algorithm. When the structure of a sample is composed of more than two phases, the subroutines (dotted line square) repeat for each one of them, in such a manner that the structure is generated in

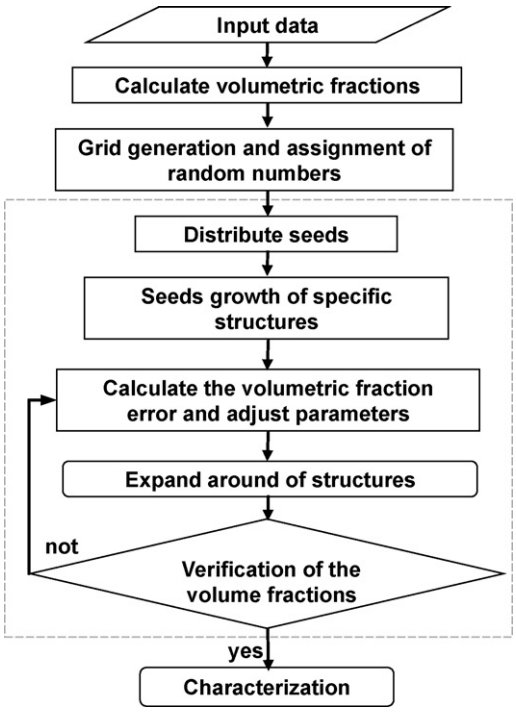

Fig. 2. General flow diagram of the microstructural reconstruction algorithm. The subroutines in the dotted line square are repeated for each reconstructed phase.

stages, where each stage corresponds to the complete generation of a phase.

The input variables in the microstructural reconstruction algorithm are: (i) platinum load (γ_{Pt}); (ii) nafion® load (β_N); (iii) weight percent of carbon-supported platinum (θ_{Pt}); (iv) total porosity and relative porosity of $n-1$ samples; (v) domain and control volume dimensions at each scale; and (vi) average size of representative elements at each scale.

The domain is fractioned in finite control volumes (FCVs), where each volume is identified by an index number randomly distributed and computer-generated by a random number generator [41].

The reconstruction method of each phase considers three formation stages: (1) the center of the representative elements at each scale (i.e. primary elements, agglomerates, mesoporous, isles, etc.) are stochastically distributed; (2) around such centers and in one single step, a previously configured specific tridimensional geometry is generated (i.e. amorphous sphere structures, ellipses, tubes, etc.); (3) in a random manner the surroundings are filled until the required volume fraction is fulfilled.

The centers of such structures are denominated seeds and the number of seeds distributed in the computing domain, is calculated using Eq. (9),

$$NS = \frac{VC_{Ti}}{VC_{Ui}} \tag{9}$$

where NS in the integer number of seed control volumes, VC_{Ti} is the number of total control volumes necessary to fulfill the volume fraction of the representative element in the whole computing domain and VC_{Ui} the number of control volumes occupied by one single representative element. The index function (I_s) that distributes the seeds has the following general form:

$$I_s(x) = \begin{cases} 1, & \text{if } 1 \le x \le NS \\ 0, & \text{otherwise} \end{cases} \tag{10}$$

The structure of representative elements is previously defined and designed pixel by pixel by a subroutine according to the known morphological features of that element, to then be systematically generated around all seeds. The growth of the surroundings of representative elements is controlled based on volume fractions as described by Eq. (11):

$$E = \frac{|V_R - V_A|}{V_R} \tag{11}$$

where E is the volume error that exist during the assignation, V_A is the assigned volume and V_R the reference volume for the specific phase. V_R is obtained for each reconstructing phase. At the "inside an agglomerate" scale, V_R is obtained by Eqs. (3), (4) and (5) for platinum, carbon and ionomer, respectively. At the "mesoporous" and "agglomerate and micropores" scales, V_R is obtained by Eq. (6). The range of available adjacent FCVs (RID) for the expansion is limited by the following function,

$$RID = VCT \exp\left(\frac{E-1}{T}\right) \tag{12}$$

where VCT is the total number of FCVs in the sample domain and T is a parameter that regulates the RID's value, this is an empirical relation used to guarantee that V_R converges to V_A. The index function (I_e) for this assignment is:

$$I_e(NI) = \begin{cases} 1, & \text{if } NI \le RID \\ 0, & \text{otherwise} \end{cases} \tag{13}$$

where NI is the random FCV's index number. After the expansion, the structure is characterized. The two-point correlation function (S_2) of a homogeneous medium can be obtained by randomly "tossing" a line segment of r length with a specific orientation and counting the number of times that the beginning (x) and the end ($x+r$) of the line fall in phase j, as described by Eq. (14):

$$S_2(x, r) = \left\langle I_j(x) I_j(x+r) \right\rangle \tag{14}$$

where the angular parenthesis refers to the statistical average when the whole domain is evaluated and I_j is equal to 1 when the point belongs to phase j as described by the following identity function:

$$I_j(x) = \begin{cases} 1, & \text{if } x \text{ is in the phase } j \\ 0, & \text{otherwise} \end{cases} \tag{15}$$

Using orthogonal coordinates, the two-point correlation function employed to characterize the generated structures becomes:

$$S_2(r) = \frac{1}{3N^2}\left[\sum_{j,k=1}^{N} S_{2,i}(r) + \sum_{k,i=1}^{N} S_{2,j}(r) + \sum_{i,j=1}^{N} S_{2,k}(r)\right] \tag{16}$$

where N is the computing domain cubic length and $S_{2,i}(r)$ is the two-point correlation function along i direction (Eq. (17)),

$$S_{2,i}(r) = \frac{1}{N-r}\sum_{i=1}^{N-r} I(i,j,k)\, I(i+r,j,k) \tag{17}$$

Similarly $S_{2,j}$ and $S_{2,k}$ can be defined.

The pore size is determined by the distribution of spheres of different radii in the porous structure, where the pore radius is equal to radius of the sphere that in its inside is formed by the "empty" phase [42]. To avoid that large spaces are fractioned into smaller spaces, the spheres' radii begin to be modified from a maximum limit to unity. The characterized spaces are identified by the following index function,

$$I_{tp}(x) = \begin{cases} 0, & \text{if } B \subseteq X \\ 1, & \text{otherwise} \end{cases} \tag{18}$$

where X represents the porous spaces and B the sphere. The maximum sphere's radius is determined by a similar function evaluated

Table 1
Dimensions of the domain and control volume for the studied scales.

Sample	$N_x = N_y = N_z$ (nm)	$d_x = d_y = d_z$ (nm)
M_3	300	3
M_2	5000	50
M_1	45,000	300

in the plane i–j along k. The pore size distribution in each sample at different scale, is defined by Eq. (19),

$$F_{r_a,M_n} = \frac{VP_{r_a,M_n}}{VP_{M_n}} \tag{19}$$

where F_{r_a,M_n} is the volume fraction that characterizes the occupied volume by pores of diameter r_a(VP_{r_a,M_n}) over the total volume occupied by the empty space (VP_{M_n}) in each of the M_n samples. For scaling, this equation can be extended to find the pore size distribution along the CL (Eq. (20)):

$$FT_{r_a}(F_{r_a,M_n}) = \frac{F_{r_a,M_n}}{\Phi_T}(\Phi_i)\prod(1-\Phi_{i-1}) \tag{20}$$

where FT_{r_a} is the volume fraction that characterizes the occupied volume by pores of diameter r_a over the total occupied volume by the empty phase in the whole CL; Φ_T is the CL's total porosity and Φ_i the sample's relative porosity. For example, when $n = 1$, $\Phi_{i-1} = 0$.

2.3. Effective ohmic conductivity

Ohm's law relates the electric current (J) of a conducting material directly to the applied voltage or potential (ΔE), as described by Eq. (21),

$$J = kA\frac{\Delta E}{L} \tag{21}$$

where k is the proportionality coefficient so-called conductivity which is a property of the material, A and L are area and length of charge transport, respectively. By applying the continuity equation in a medium discretized by FCV, the charge conservation transport equation in a non-reactive system can be expressed by Eq. (22):

$$\nabla\cdot(k_m\nabla\phi_e) = 0 \tag{22}$$

where k_m is the material's conductivity and ϕ_e the applied potential. By solving the charge transport continuity equation directly in the structural mesh, it is possible to obtain the average of all local current flows (J_a), generated by the potential. Taking Eq. (21) and substituting J_a, we can obtain the effective length to area of conduction ratio ($L_{meff}/A_{meff} = k(\phi_e/J_a)$). As it will be shown later, this method, will simplify the structure scaling.

Table 2
Porosity of simulated structures.

Φ_T (%)	Φ_Φ (%)	Φ_{M_1} (%)	Φ_{M_2} (%)
0.50	D1	7.50	45.95
0.50	D2	10.00	44.44
0.50	D3	12.50	42.86
0.50	D4	15.00	41.18
0.40	D1	6.00	36.17
0.40	D2	8.00	34.78
0.40	D3	10.00	33.33
0.40	D4	12.00	31.82
0.30	D1	4.50	26.70
0.30	D2	6.00	25.53
0.30	D3	7.50	24.32
0.30	D4	9.00	23.08
0.20	D1	3.00	17.53
0.20	D2	4.00	16.67
0.20	D3	5.00	15.79
0.20	D4	6.00	14.89

The effective resistance (R_{eff}) of a heterogeneous material, composed by a conductive phase and one or more insulating phases, is a function of the conductive material's resistivity (ρ_m), its effective area (A_{meff}) and its effective length (L_{meff}) as described in the following equation,

$$R_{eff} = \rho_m\frac{L_{meff}}{A_{meff}} \tag{23}$$

From a different angle, the R_{eff} can be calculated as a function of the effective resistivity (ρ_{meff}) and the input data: area of the sample (A_m) and length of the sample (L_m), as described by Eq. (24),

$$R_{eff} = \rho_{meff}\frac{L_m}{A_m} \tag{24}$$

Using Eqs. (23) and (24) we can obtain ρ_{meff}, which relates the effective resistivity of the whole sample with the resistivity, effective length and effective area of conduction of the conductive phase, Eq. (25),

$$\rho_{meff} = \left(\rho_m\frac{L_{meff}}{A_{meff}}\right)\frac{A_m}{L_m} \tag{25}$$

As the effective resistivity characterizes the material by being an intensive property and being able to be extended to find the resistance of any continuous structure formed by the same material, this equation can be generalized to find the resistivity of an element formed by subdomains of smaller scales (Eq. (26)):

$$\rho_{meff_T} = \rho_m\prod_{i=1}^{n}\frac{L_{meff_i}}{A_{meff_i}}\prod_{i=1}^{n}\frac{A_{m_i}}{L_{m_i}} \tag{26}$$

where ρ_{meff_T} is the effective resistivity of the global domain formed by various smaller scale subdomains i; L_{meff_i} is the effective length and A_{meff_i} is the effective area of the phase under study in every subdomain. L_{m_i} is the length and A_{m_i} is the area of the sample of every subdomain.

To normalize and generalize results, in this work calculated resistivities are used to estimate a conduction efficiency (ε_k). As conductivity is the inverse of resistivity, the CL's effective conductivity is the inverse of the effective resistivity value $k_{meff_T} = \rho_{meff_T}^{-1}$. ε_k is calculated by comparing the effective conductivity with the nominal conductivity, as described by Eq. (27). By substituting Eq. (26) in Eq. (27), we can obtain a relation that provides the conduction efficiency of the global domain (ε_{k_T}) which is formed by several subdomains of smaller scale (Eq. (28)),

$$\varepsilon_k = \frac{k_{meff}}{k_m} \tag{27}$$

$$\varepsilon_{k_T} = \prod_{1}^{n}\frac{A_{meff_i}}{L_{meff_i}}\prod_{1}^{n}\frac{L_{m_i}}{A_{m_i}} \tag{28}$$

For example, to study the conduction efficiency with three scaling levels the equation would be:

$$\varepsilon_{k_T} = \left(\frac{A_{meff_1}A_{meff_2}A_{meff_3}}{L_{meff_1}L_{meff_2}L_{meff_3}}\right)\left(\frac{L_{m_1}L_{m_2}L_{m_3}}{A_{m_1}A_{m_2}A_{m_3}}\right) \tag{29}$$

Although in this work only the ohmic conduction efficiency will be determined, other transport properties, such as thermal conductivity and diffusion coefficient, just to mention a couple of them, could be determined under the same approach.

3. Simulation conditions

In this work we will determine the electronic and ionic conduction efficiency of a CL with different structural features: (1) ionomer electrode load (β_N) in the range of 20–80%$_{wt}$; (2) CL porosity in

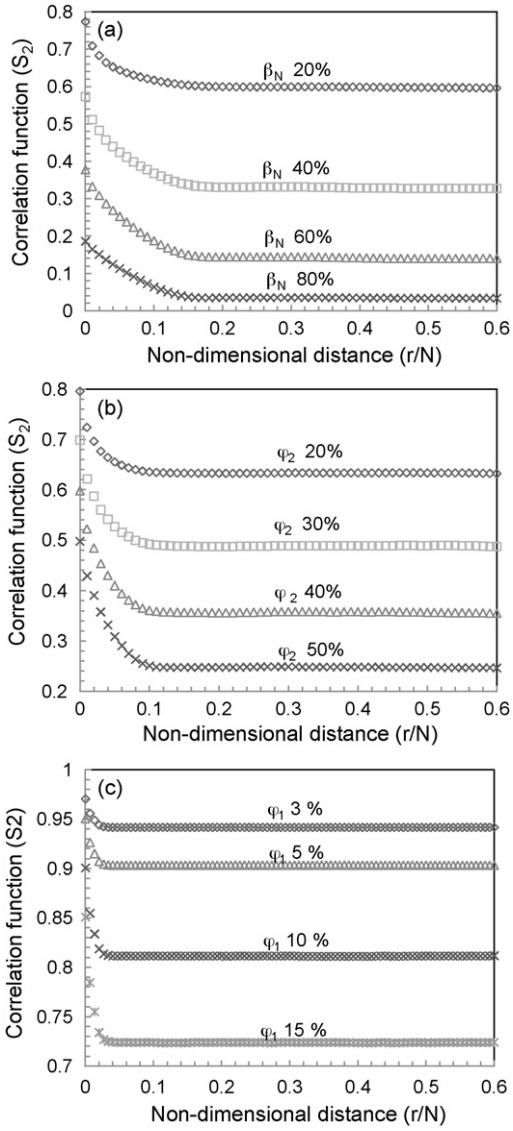

Fig. 3. Two-point correlation function (S_2) versus a non-dimensional distance (r/N) for some representative structures at each studied scale. (a) shows S_2 for the carbon phase at the M_3 scale, where each curve corresponds to different ionomer loads (β_N); (b) shows S_2 for the agglomerates at the M_2 scale; and (c) shows S_2 for the pseudo-solid phase at the M_1 scale. In (b) and (c) each curve corresponds to different porosities (Φ_i).

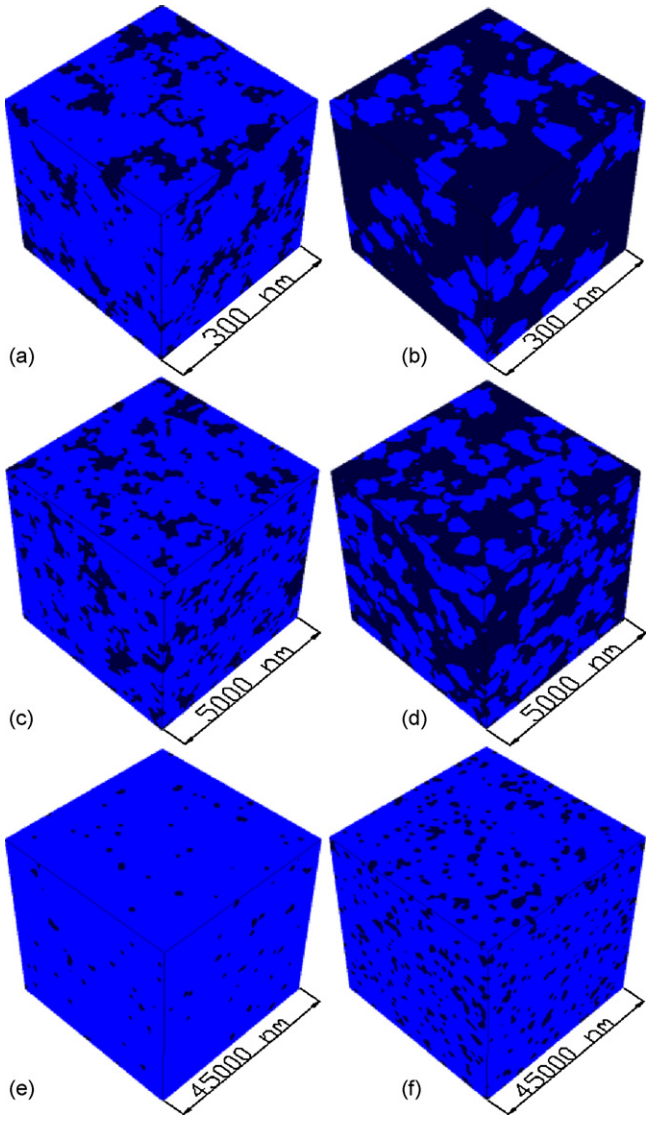

Fig. 4. Images of some reconstructed samples. (a) and (b) represent the M_3 scale, with β_N equal to 20 and 60%, respectively, the blue color represents the carbon phase and dark blue the ionomer phase. (c) and (d) represent the M_2 scale, with Φ_{M_2} equal to 20 and 50%, respectively, the blue color represents the agglomerates and dark blue the empty phase. (e) and (f) show the M_1 scale with Φ_{M_1} equal to 3 and 15%, respectively, here the blue color represents the pseudo-solid phase and dark blue the empty phase. (For interpretation of the references to color in this figure legend, the reader is referred to the web version of the article.)

the range of 20–50% and (3) pore size distribution by modification of the relative porosity. All generated structures have the following characteristics: 20%$_{wt}$ Pt/C; 0.5 mg Pt cm^{-2}; average Pt particle diameter, C diameter (ER_C), agglomerate diameter (ER_M) and mesopore diameter (ER_P) of 3 nm, 50 nm, 500 nm and 600 nm, respectively. Density of materials forming the solid structure: Pt, C and ionomer are 21,450, 1800 and 2000 mg cm^{-3}, respectively. Each one of the resulting structures is generated 10 times by different random series and then their values are averaged.

Every CL is then studied at three different scales, namely:

(a) Inside an agglomerate (M_3), the phase's reconstruction sequence in the computing domain is: (i) carbon agglomerate generation, (ii) platinum on carbon placement-generation, and (iii) the rest is ionomer.
(b) Agglomerates and micropores (M_2), the reconstruction sequence is: (i) agglomerate generation and (ii) the rest is empty room.
(c) Mesopores (M_1), reconstruction sequence is: (i) mesopore generation and (ii) the rest is a pseudo-solid structure.

Table 1 briefs the dimension of the computing domain (N_x, N_y and N_z) and the FCVs (d_x, d_y and d_z) for each of the scales (M). These values are based on average diameters of representative elements of the already mentioned scaling method.

In this work the pore size distribution is controlled indirectly by defining the relative porosity of the so-called "mesoporous" scale (Φ_{M_1}) as a percentage of total porosity (Eq. (30)),

$$\Phi_\Phi = \frac{\Phi_{M_1}}{\Phi_T} \tag{30}$$

where Φ_Φ is the total porosity percentage assigned to Φ_{M_1} and Φ_T is the total electrode porosity. From a physical point of view, Φ_Φ is directly proportional to the pore size distribution because it determines the volume occupied by mesopores. It is worth men-

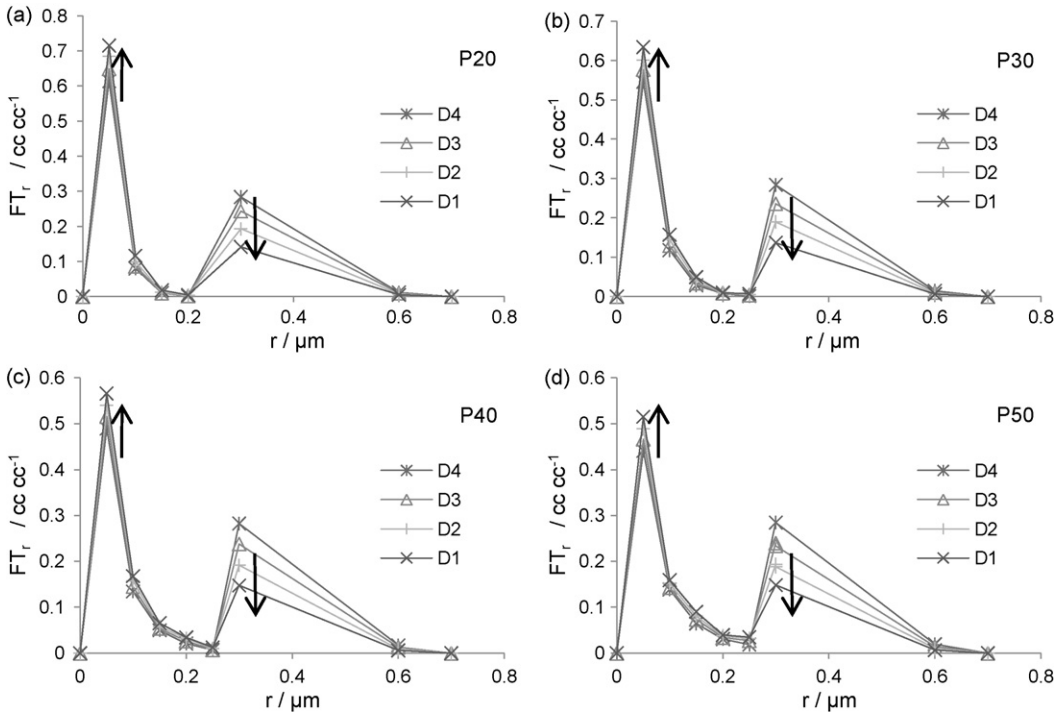

Fig. 5. Pore size distribution of reconstructed catalyst layers. (a), (b), (c) and (d) correspond to 20, 30, 40, and 50% of total porosity (Φ_T), respectively. The arrows show how Φ_Φ is modified.

tioning that the relative porosity of the M_2 scale is conditioned by Eq. (8). Table 2 specifies relative porosities used in this work, where D1, D2, D3 and D4 refer to Φ_Φ equal to 0.15, 0.20, 0.25 and 0.30, respectively.

4. Results and discussion

The present methodology proposes the study of the following CLs: 4 porosities, 4 pore size distributions and 13 different ionomer loads (from 20 to 80 in steps of 5%). As each structure will be generated by ten different random series we will have a total of 2080 analyzed structures. Using one single personal computer with 3 Gb of RAM memory and a 2.4 GHz processor, the computing time is of approximately 100 h, with the use of scaling, not including the time for establishing the problem and for the analysis of results. The scaling method not only reduces computer processing time but also allows a detailed study of the CL at the nanoscale level. The domain lattice of the cubic simple simulating the CL (M_1) is 45,000 nm, while the lattice of the sample's control volume detailing the inside of an agglomerate (M_3) is 3 nm. Without the scaling technique, the computing domain would need to be generated by 3.375×10^{12} control volumes, which would make it impossible to do with the previously mentioned computer.

4.1. Characterization of reconstructed structures

Fig. 3 shows the two-point correlation function (S_2) obtained for some representative structures at each studied scale. These values are plotted versus a non-dimensional distance r/N, where r is the distance between two points and N the domain lattice. In Fig. 3(a) S_2 is shown when the carbon phase is analyzed at the M_3 scale. Each curve corresponds to a different ionomer loading (β_N). In Fig. 3(b) and (c), S_2 is calculated for the "pseudo-solid" phase at the M_2 and M_1 scales, respectively. In these last two figures, each curve corresponds to different relative porosities. When $r = 0$, S_2 represents the volume fraction of the characterized phase. All correlation functions (S_2) decay exponentially down to the squared volume fraction, where its value is independent of r.

Fig. 4 shows representative images of reconstructed scales corresponding to S_2 in Fig. 3. Fig. 4(a) and (b) correspond to the M_3 scale, with a β_N of 20 and 60%$_{wt}$, respectively, where the blue color represents the carbon phase and dark blue the ionomer phase. Fig. 4(c) and (d) correspond to the M_2 scale, with Φ_{M_2} of 20 and 50%, respectively, where the blue color represents the agglomerates and dark blue the empty phase. Fig. 4(e) and (f) show the M_1 scale with Φ_{M_1} 3 and 15%, respectively, here the blue color represents the pseudo-solid phase and dark blue the empty phase. In general the reconstructed structures look alike in the three planes for each shown condition. Also at each scale it is clear the effect of extreme values of: ionomer load at the M_3 scale (Fig. 4(a) and (b)) and relative porosity at M_2 (Fig. 4(c) and (d)) and M_1 (Fig. 4(e) and (f)) scales.

The pore size distribution in the CL is obtained using Eq. (20). The resulting expressions, where only two samples contain the empty phase, are:

$$FT_{r_a}(F_{r_a,M_1}) = \frac{F_{r_a,M_1}}{\Phi_R}(\Phi_1) \tag{31}$$

$$FT_{r_a}(F_{r_a,M_2}) = \frac{F_{r_a,M_2}}{\Phi_R}(\Phi_2)(1-\Phi_1) \tag{32}$$

Fig. 5 shows the pore size distribution results calculated. Fig. 5(a), (b), (c) and (d) correspond to 20, 30, 40, and 50% of total porosity, respectively, for a hypothetical CL. In these plots one can observe the pore size variation by normalizing Φ_Φ. From that figure it can be seen that when Φ_Φ decreases, the frequency of the ~50 nm pore size (left peak) increases while the frequency of the ~300 nm pore size (right peak) diminishes. An example of this behavior is seen in Fig. 5(a) when $\Phi_\Phi = 0.30$ (D4), $FT_{r_{50}} = 0.61$ and $FT_{r_{300}} = 0.28$ and when $\Phi_\Phi = 0.15$ (D1), $FT_{r_{50}} = 0.71$ and $FT_{r_{300}} = 0.14$. The arrows in those figures point it out. These results are expected as Φ_Φ is directly proportional to the relative porosity of sample with a larger scale, therefore when its value decreases the volume of those pores

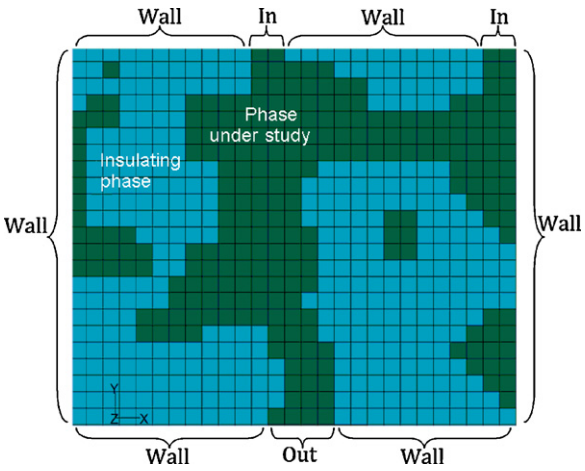

Fig. 6. Schematics of the general boundary conditions for the charge transport simulation of the cases studied at the different scales.

with larger size decrease. These results confirm that the pore size distribution of the CL was modified by the control of Φ_Φ. Such distribution shows two peaks (at 0.05 μm and 0.3 μm), which are strongly influenced by the carbon particle size and the mesopore size both introduced as input data.

4.2. Electric and ionic transport coefficients

Fig. 6 shows the general boundary conditions (in 2D) used during simulation of the cases studied at the different scales. As the structures are homogeneous, the side of the cubic domain that will be assigned to the "flow current input" is not relevant, but clearly the output should be located at the opposite side. At the input side, a 1.1 V potential is specified exclusively on the FCV of the phase under study, while in the faces of FCV of the isolating phase the boundary condition is a zero current flow. At the output a 1.0 V potential is specified only for the phase under study, therefore having a 0.1 V gradient. Other sides in the cubic domain are specified with a zero current flow condition. It must be mentioned that these limiting values have the only purpose of determining the conduction efficiency and do not represent actual voltage distribution on the different scales at the same time.

As the material's resistivity does not affect results of the conduction efficiency (Eq. (28)), the phase under study is specified with an arbitrary high conductivity (1000 S m^{-1}) while the isolating phase with an arbitrary low conductivity (0.0001 S m^{-1}). At the M_1 scale the phase under study is the pseudo-solid, at the M_2 scale the phase being studied is the agglomerates and at both M_1 and M_2 scales, the insulating phase corresponds always to the empty phase. To determine the ionic conduction efficiency, the phase under study at the M_3 scale is the ionomer and the insulating phase corresponds to both carbon and platinum. To determine the electronic conduction efficiency, the phase under study at the M_3 scale corresponds to carbon and platinum, while the insulating phase is the ionomer.

Fig. 7 shows the potential distribution in volts within the electronic conduction phase for reconstructed CLs shown in Fig. 4. The potential distribution is estimated using the boundary conditions previously mentioned, while the current flows are used exclusively to calculate the conduction efficiency. The domains of Fig. 7(a)–(f) are limited by an imaginary line and the potential distribution is plotted exclusively in the electronic conduction phase.

Fig. 8 plots proton (a) and electronic (b) conduction efficiency versus different ionomer loadings in reconstructed CLs with 30% total porosity, where each curve represents a different pore size distribution. In that figure it can be observed that the proton

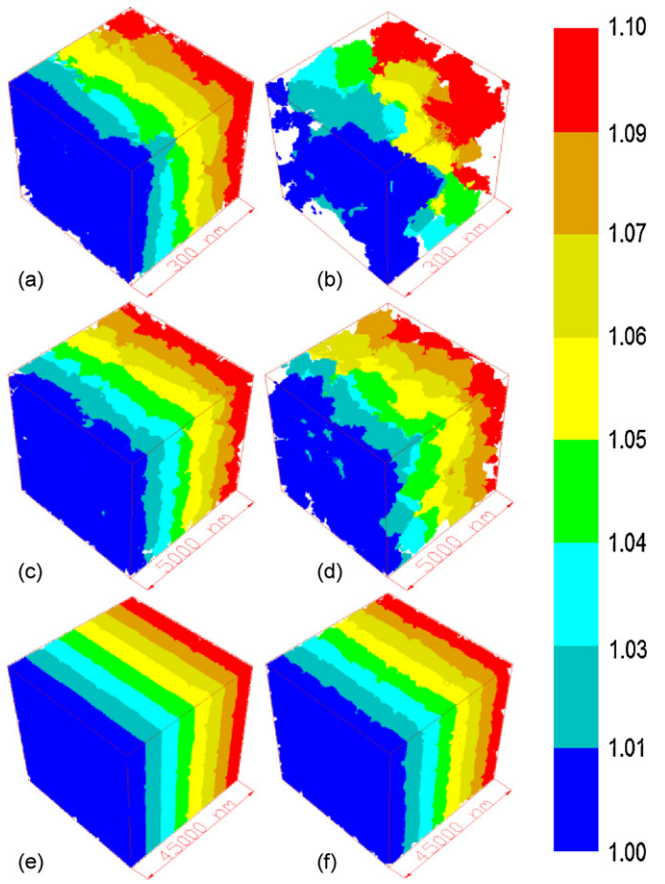

Fig. 7. Potential distribution (V) of the electronic conduction phase of some reconstructed samples. (a) and (b) show potential distribution for the M_3 scale, with β_N equal to 20 and 60%, respectively. (c) and (d) show the potential distribution for the M_2 scale, with Φ_{M_2} equal to 20 and 50%, respectively. (e) and (f) show the potential distribution for the M_1 scale with Φ_{M_1} equal to 3 and 15%, respectively.

conduction efficiency increases, while the electronic conduction efficiency diminishes, both in an exponential fashion, when β_N increases. This is an expected behavior as when β_N grows what really increases is the volume fraction of the ionomer phase while the electronic conduction phase decreases inversely. On the other hand, it is relevant to point out that the pore size distribution does not affect the effective ionic or the effective electronic conduction for the same β_N value.

In Fig. 9 we show results obtained for proton (a) and electronic (b) conduction efficiency versus different total porosity in reconstructed CLs now with 35% of ionomer loading. Each curve represents a different pore size distribution and it can be noted that both efficiencies electronic and ionic conduction decrease almost linearly when the CL's porosity increases. This trend is caused by the smaller volume proportion of solid components (electronic and ionic) when the porosity increases, which clearly affects the effective conductivity of the heterogeneous material. Also it should be noticed that the slope for the electronic efficiency is different from that for the ionic efficiency. As we shall see later, the decay rate depends on β_N. It can be noticed from these figures that the pore size distribution does not affect the effective ionic or the effective electronic conduction for the same β_N value.

Finally, in Fig. 10 results obtained for the same properties as a function of porosity are shown. As the pore size distribution does not affect these results, conduction efficiency dependent on the pore size distribution were averaged to be included in this analysis. Besides the before mentioned trends, one can also observe that the

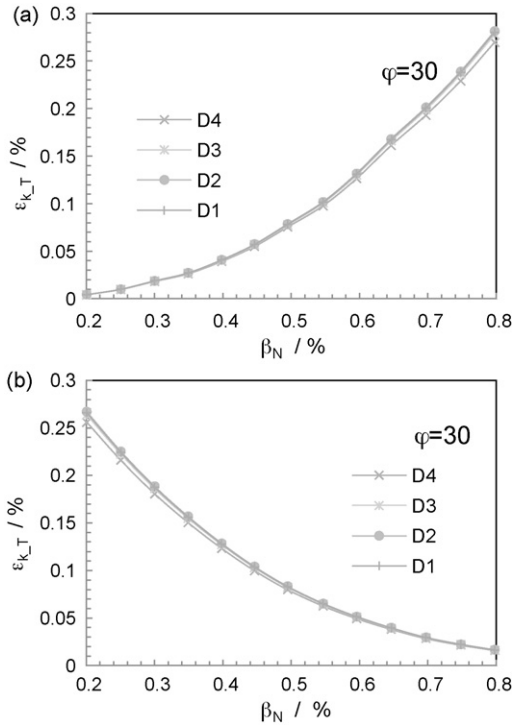

Fig. 8. Effect of ionomer load (β_N) on proton conduction (a) and electronic conduction (b) efficiency of the reconstructed CLs with 30% porosity (Φ_T). Each curve represents different pore size distribution.

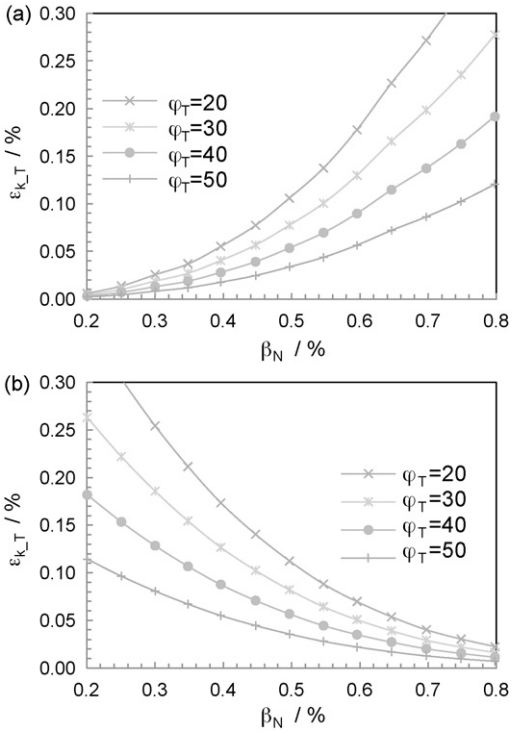

Fig. 10. Effect of ionomer load (β_N) on proton conduction (a) and electronic conduction (b) efficiency of the reconstructed CLs. Each curve represents different porosities (Φ_T). The effect of the pore size distribution was averaged.

decay rate of the proton conduction efficiency increases, while the electronic conduction efficiency diminishes when β_N increases.

For the experimental validation of the present method the following must be considered: (i) The microstructure reconstruction, at each scale, should be made by a procedure that statistically ensures the correct representation of the experimental structure. (ii) The experimental effective transport coefficients should be exclusive to the CL. This information is not currently available in the literature. Nevertheless Boyer et al. [43] conducted an experimental study where the proton conductivity of a pseudo-CL is similar to the results presented in this paper. It is noteworthy that experimental validation is a current work in our laboratory and will be published in the near future.

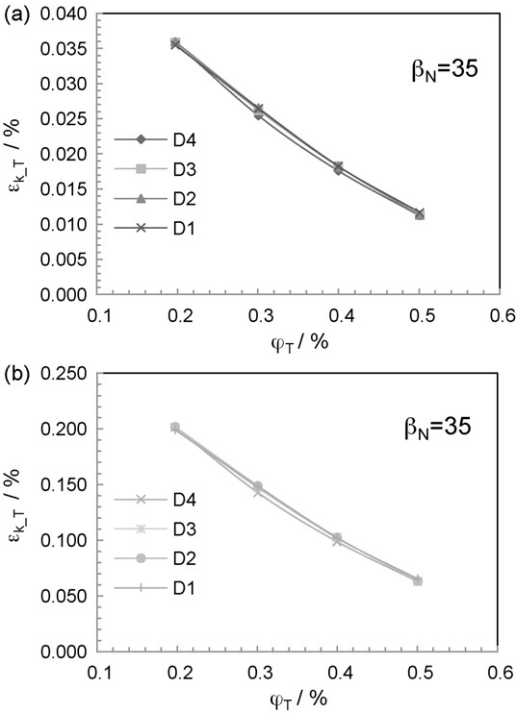

Fig. 9. Effect of porosity (Φ_T) on proton conduction (a) and electronic conduction (b) efficiency of the reconstructed CLs with 35% ionomer load (β_N). Each curve represents different pore size distribution.

5. Conclusions

A technique to determine the effective electronic and ionic conduction of a catalyst layer in a PEM fuel cell has been proposed. The scaling approach can be applied to determine other effective transport parameters of heterogeneous structures in CLs. The mathematical relationships can be systematically applied to determine effective coefficients of other processes such as thermal conduction and mass diffusion. The proposed mesh generation algorithm makes use of available information before and after the CL fabrication and the generated structures are characterized by two-point correlation functions and pore size distributions. The scaling approach significantly reduces the computing hardware requirement for the detailed study of nanoscale structures. Finally, the techniques presented in this work can be applied to study already existent CL microstructures as well as to propose new and more efficient CLs.

References

[1] K. Adamson, Energy Policy 32 (2004) 1231–1242.
[2] G.W. Crabtree, M.S. Dresselhaus, M.V. Buchanan, Phys. Today 57 (2004) 39–44.
[3] A.C. Lloyd, J. Power Sources 86 (2000) 57–60.
[4] Y.-H. Cho, H.-S. Park, Y.-H. Cho, D.-S. Jung, H.-Y. Park, Y.-E. Sung, J. Power Sources 172 (2007) 89–93.
[5] T. Romero-Castañon, L.G. Arriaga, U. Cano, J. Power Sources 118 (2003) 179–182.

[6] M. Uchida, Y. Fukuoka, Y. Sugawara, N. Eda, A. Ohta, J. Electrochem. Soc. 143 (1996) 2245–2252.
[7] P. Gode, F. Jaouen, G. Lindbergh, A. Lundblad, G. Sundholm, Electrochim. Acta 48 (2003) 4175–4187.
[8] R. Flückiger, S.A. Freunberger, D. Kramer, A. Wokaun, G.G. Scherer, F.N. Büchi, Electrochim. Acta 54 (2008) 551–559.
[9] Q. Wang, M. Eikerling, D. Song, Z. Liu, J. Electroanal. Chem. 573 (2004) 61–69.
[10] K. Broka, P. Ekdunge, J. Appl. Electrochem. 27 (1997) 281–289.
[11] S. Kamarajugadda, S. Mazumder, J. Power Sources 183 (2008) 629–642.
[12] Q. Yan, J. Wu, Energy Convers. Manage. 49 (2008) 2425–2433.
[13] F. Scheiba, N. Benker, U. Kunza, C. Rotha, H. Fuess, J. Power Sources 177 (2008) 273–280.
[14] J. Xie, D.L. Wood III, K.L. More, P. Atanassov, R.L. Borup, J. Electrochem. Soc. 152 (2005) A1011–A1020.
[15] M. Secanell, K. Karan, A. Suleman, N. Djilali, Electrochim. Acta 52 (2007) 6318–6337.
[16] A.A. Shah, G.-S. Kim, W. Gervais, A. Young, K. Promislow, J. Li, S. Ye, J. Power Sources 160 (2006) 1251–1268.
[17] S.H. Kim, H. Pitsch, J. Electrochem. Soc. 156 (2009) B673–B681.
[18] W. Sun, B.A. Peppley, K. Karan, Electrochim. Acta 50 (2005) 3359–3374.
[19] S. Torquato, Random Heterogeneous Materials: Microstructure and Macroscopic Properties, Springer-Verlag, New York, 2002.
[20] P.K. Das, X. Li, Z.-S. Liu, Appl. Energy 87 (2010) 2785–2796.
[21] J. Maxwell-Garnett, Philos. Trans. R. Soc. London Ser. A 203 (1904) 385–420.
[22] D. Bruggeman, Ann. Phys. (Leipzig) 24 (1935) 636–679.
[23] J.A. Quiblier, J. Colloid Interface Sci. 98 (1984) 84–102.
[24] P. Capek, V. Hejtmánek, L. Brabec, A. Zikánová, M. Kocirík, Transp. Porous Media 76 (2009) 179–198.
[25] E. Patelli, G. Schuëller, Comput. Mater. Sci. 45 (2009) 536–549.
[26] Y. Jiao, F.H. Stillinger, S. Torquato, Phys. Rev. E 77 (2008) 031135.1–031135.15.
[27] X. Zhao, J. Yao, Y. Yi, Transp. Porous Media 69 (2007) 1–11.
[28] J.-H. Jang, W.-M. Yan, H.-Y. Li, W.-C. Tsai, Int. J. Hydrogen Energy 33 (2008) 156–164.
[29] J.-K. Kuo, T.-H. Yen, C.-K. Chen, J. Power Sources 177 (2008) 96–103.
[30] F.-B. Weng, A. Su, G.-B. Jung, Y.-C. Chiu, S.-H. Chan, J. Power Sources 145 (2005) 546–554.
[31] T.E. Springer, I.D. Raistrick, J. Electrochem. Soc. 136 (1989) 1594–1603.
[32] N.P. Siegel, J. Power Sources 115 (2003) 81–89.
[33] L. Matamoros, D. Bruggemann, J. Power Sources 172 (2007) 253–264.
[34] G. Wang, P.P. Mukherjee, C.-Y. Wang, Electrochim. Acta 51 (2006) 3151–3160.
[35] M.S. Wilson, U.S. Pat. No. 5,234,777 (1993).
[36] S. Litster, G. McLean, J. Power Sources 130 (2004) 61–76.
[37] B. Escobar, S.A. Gamboa, U. Pal, R. Guardián, D. Acosta, C. Magaña, X. Mathew, Int. J. Hydrogen Energy 35 (2010) 4215–4221.
[38] J. Ledesma-García, R. Barbosa, T.W. Chapman, L.G. Arriaga, Luis A. Godínez, Int. J. Hydrogen Energy 34 (2009) 2008–2014.
[39] R. Barbosa, I. Gatto, G. Squadrito, G. Orozco, L.G. Arriaga, R. Ornelas, V. Antonucci, E. Passalacqua, ECS Trans. 11 (2007) 1527–1533.
[40] E. Passalacqua, F. Lufrano, G. Squadrito, A. Patti, L. Giorgi, Electrochim. Acta 46 (2001) 799–805.
[41] M. Matsumoto, T. Nishimura, ACM Trans. Modell. Comput. Simul. 8 (1998) 3–30.
[42] V.P. Schulz, J. Becker, A. Wiegmann, P.P. Mukherjee, C.Y. Wang, J. Electrochem. Soc. 154 (2007) B419–B426.
[43] C. Boyer, S. Gamburzev, O. Velev, S. Srinivasan, A.J. Appleby, Electrochim. Acta 43 (1998) 3703–3709.